POSTN^{+} cancer-associated fibroblasts determine the efficacy of immunotherapy in hepatocellular carcinoma

Hao Wang [1, 2, ‡], Yuan Liang [2, 4, ‡], Zheng Liu [5, ‡], Rui Zhang [2], Jiashuo Chao [1, 2], Mingming Wang [1, 2], Mu Liu [2], Lei Qiao [2], Zhengfeng Xuan [2], Haitao Zhao [1,*], Ling Lu [2, 3,*]

[1] Department of Liver Surgery, State Key Laboratory of Complex Severe and Rare Diseases, Peking Union Medical College Hospital, Chinese Academy of Medical Sciences and Peking Union Medical College (CAMS & PUMC), Beijing, China.

[2] Hepatobiliary Center of The First Affiliated Hospital, Nanjing Medical University; Research Unit of Liver Transplantation and Transplant Immunology, Chinese Academy of Medical Sciences, Nanjing, China.

[3] Affiliated Hospital of Xuzhou Medical University, Xuzhou, China.

[4] School of Biological Science & Medical Engineering, Southeast University, Nanjing, China.

[5] Department of General Surgery, the First Affiliated Hospital of Nanjing Medical University, Nanjing, China.

[‡] These authors contributed equally to this work

[*]Corresponding author.

Correspondence to Professor ling lv; Hepatobiliary Center of The First Affiliated Hospital, Nanjing Medical University; Research Unit of Liver Transplantation and Transplant Immunology, Chinese Academy of Medical Sciences, No. 300 Guangzhou Road, Nanjing 210029, China. Email: lvling@njmu.edu.cn.

Correspondence to Professor Haitao Zhao; Department of Liver Surgery, State Key Laboratory of Complex Severe and Rare Diseases, Peking Union Medical College Hospital, Chinese Academy of Medical Sciences and Peking Union Medical College (CAMS & PUMC), No. 1, Shuaifuyuan, Dongcheng District, Beijing 100730, China. E-mail: zhaoht@pumch.cn.

Content: Supplemental Figures 1-9

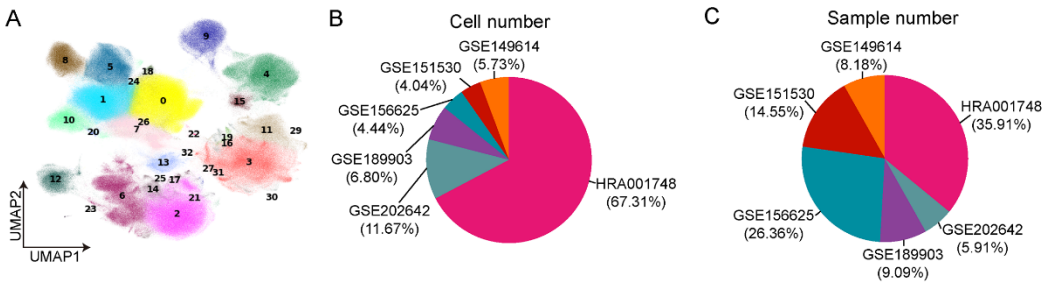

Supplementary Figure 1. The containing cohorts and cluster information.

(A) UMAP plot showing the distribution of the specific clusters. Dots represent individual cells. (B) Pie chart showing the number of cells included in our study. The different colors represent different studies. (C) Pie chart showing the sample number of our study. The different colors represent different studies.

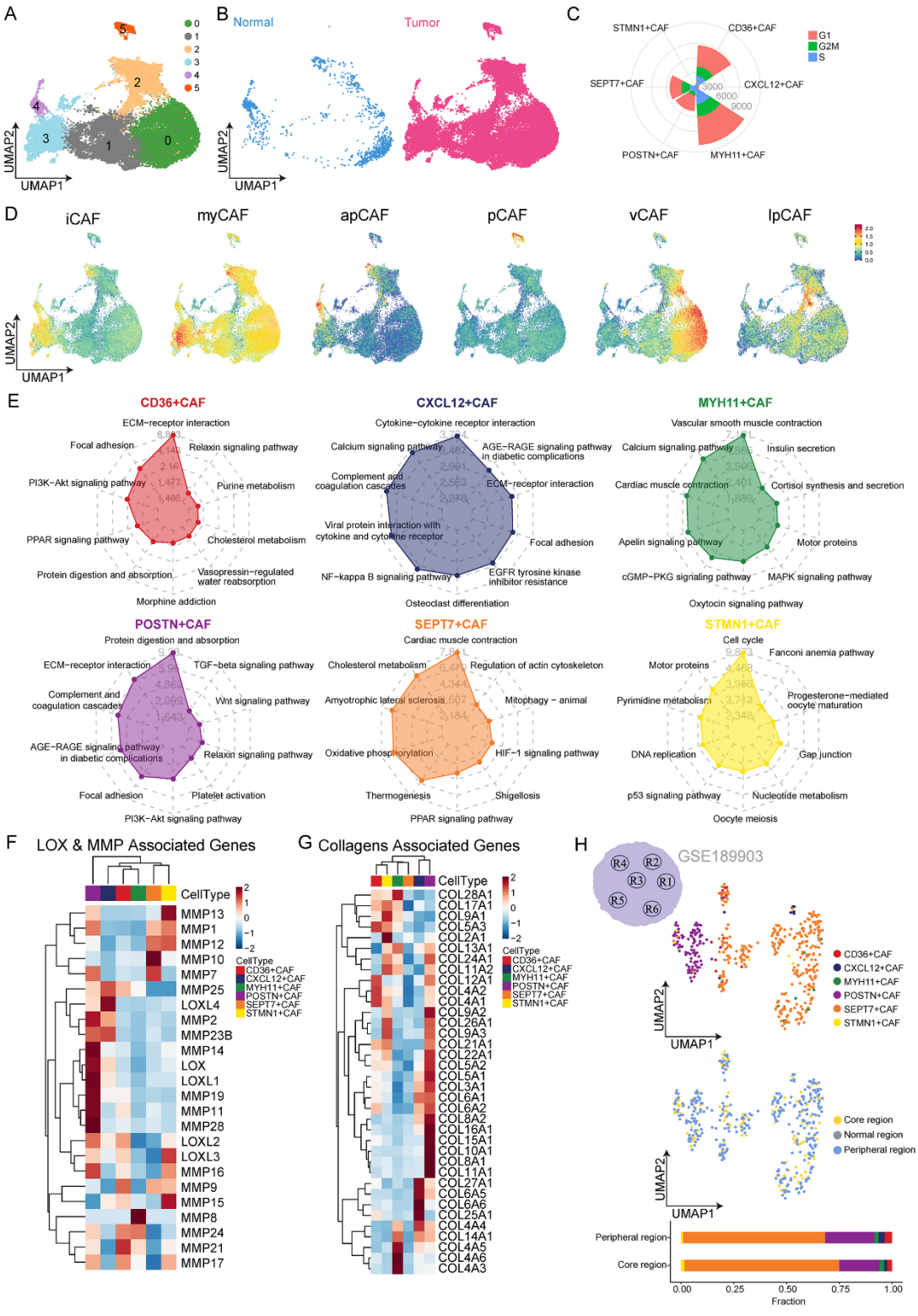

Supplementary Figure 2. CAF re-clustering analysis in HCC.

(A) UMAP plot showing the distribution of the CAF clusters. Dots represent individual cells. The different colors represent different clusters. (B) UMAP plots showing the distribution of

the CAF clusters in normal (left) and tumor (right) samples. (C) Radar plot showing the distribution of the cell cycle state in each CAF subtype. (D) UMAP plots showing the distribution of scores of six CAF phenotypes. (E) Radar plots showing KEGG terms of differentially expressed genes significantly enriched in each CAF subtype. (F-G) Heatmap showing the mean expression of lipoxygenase (LOX)- and matrix metalloproteinase (MMP) associated genes (F) and collagen (COL)-associated genes (G) in each CAF subtype. (H) UMAP plots showing the specific CAF subtypes (up) and spatial organization (middle) of CAF subtypes according to Sharma's scRNA-seq dataset. Bar plot showing the fraction of CAF subtypes in the core and peripheral regions in HCC tumors (bottom).

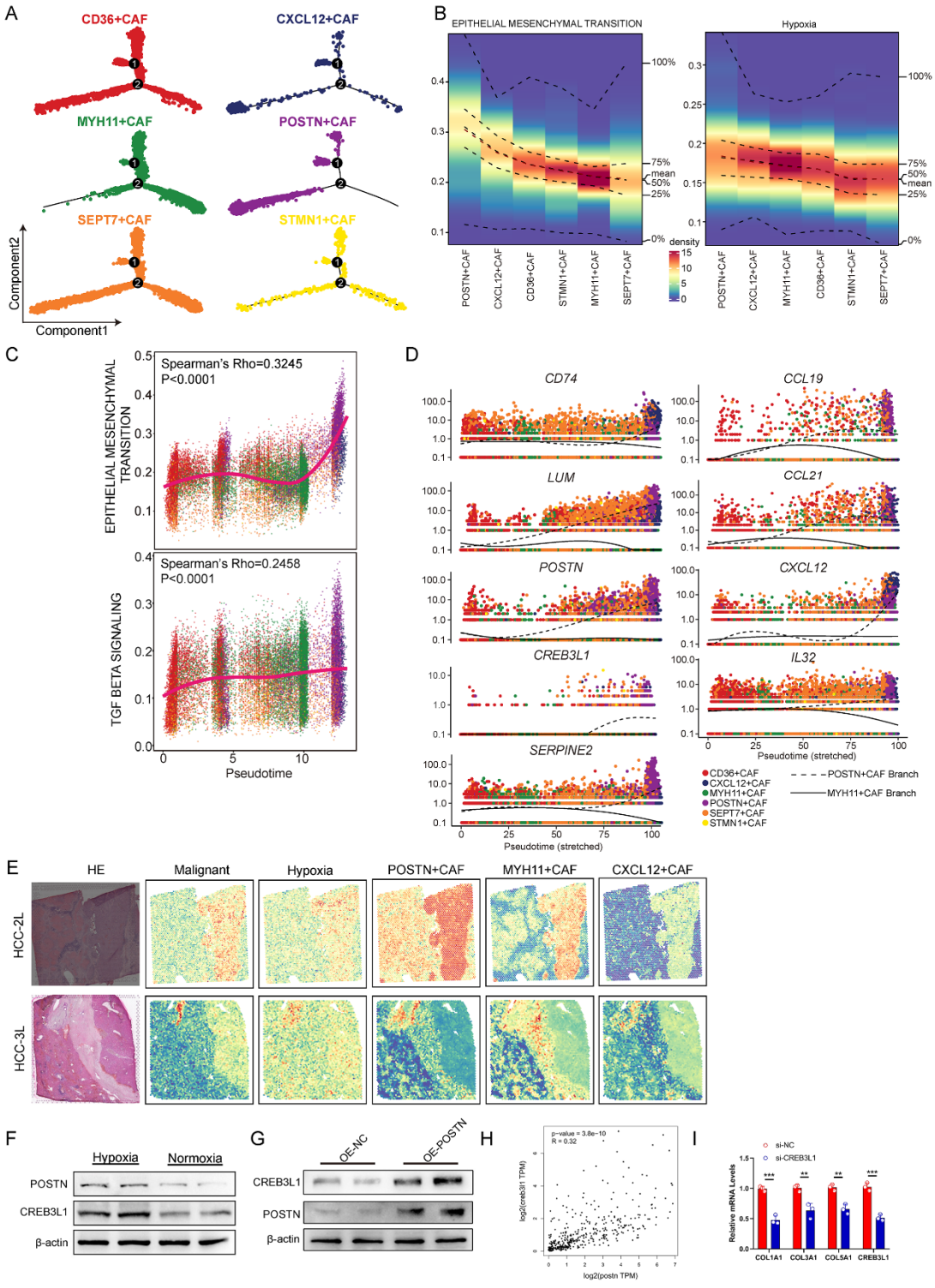

Supplementary Figure 3. Pseudotime analysis of CAF subtypes in HCC.

(A) The developmental trajectory of CAFs cells is inferred by the monocle2 subtype, which is influenced by different CAF subtypes. The different colors represent different CAF subtypes.

(B) Density heatmaps showing the density of epithelial mesenchymal transition (left) and hypoxia (right) scores for each CAF subtype. (C) Dot plots showing the Spearman's correlation of the pseudotime and epithelial mesenchymal transition scores (up), or the TGF-beta signaling score (bottom). The different colors represent different CAF subtypes. (D) Pseudotime projections of transcriptional changes in *CD74*, *LUM*, *POSTN*, *SEPRINE2*, *CCL19*, *CCL21*, *CXCL12*, *CREB3L1*, and *IL32* between the two trajectory branches. (E) The Spatial HE staining and spatial feature plots of the signature scores of malignant cells, hypoxic cells, $POSTN^+$ CAFs, $MYH11^+$ CAFs, and $CXCL12^+$ CAFs in HCC-2L and HCC-3L sections (from left to right). (F) Western blot analysis indicated that the protein levels of POSTN and CREB3L1 in CAFs under normoxia (20% O2) or hypoxia (1% O2). (G) Western blot analysis showing the protein levels of POSTN and CREB3L1 in CAFs overexpressing POSTN (OE-POSTN-CAFs) and in the control group (OE-NC-CAFs). (H) POSTN expression was correlated with CREB3L1 expression in the TCGA-LIHC cohort. (I) COL1A1, COL3A1, COL5A1, and CREB3L1 levels were examined by qRT–PCR analysis (n=3). **, $p < 0.01$. ***, $p < 0.001$.

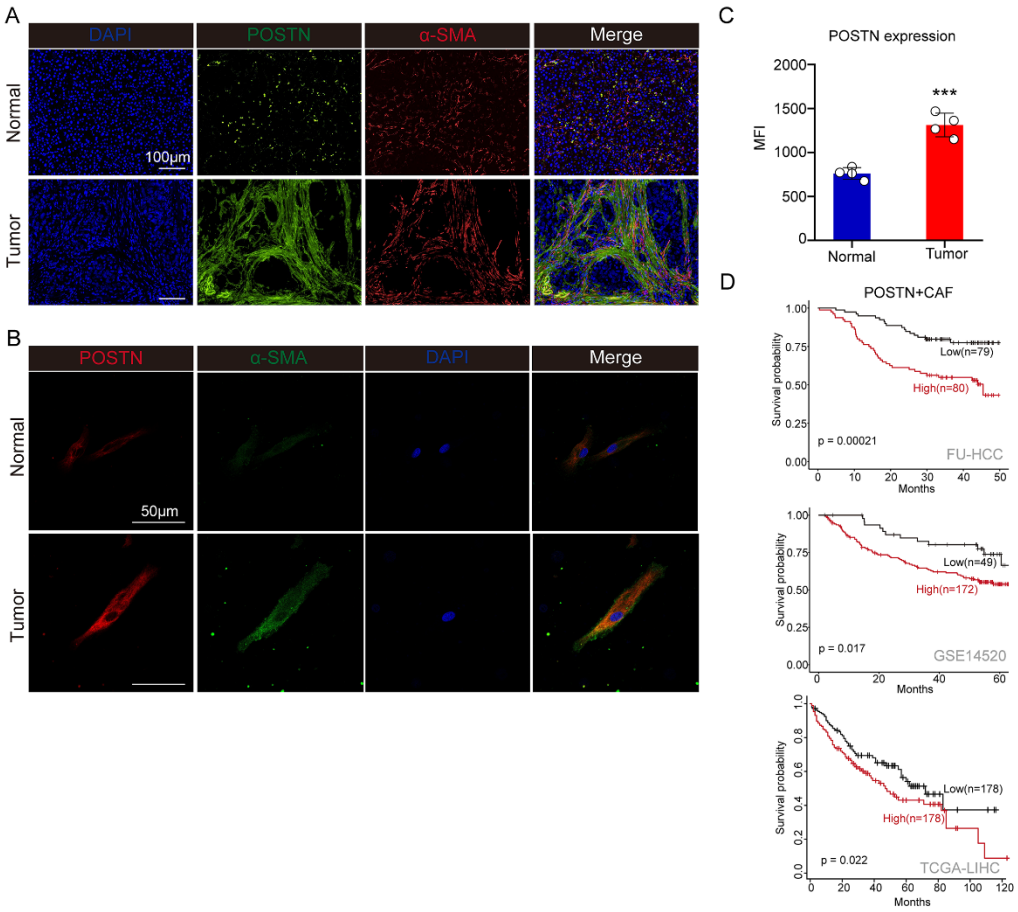

Supplementary Figure 4. Tumor-infiltrating POSTN$^+$ CAFs influence patient survival prognosis.

(A) Representative IF staining of tumor and nontumor tissues. DAPI (blue), POSTN (green), and α-SMA (red) in individual and merged channels are shown. Bar, 100 μm. (B) Comparison of the mean fluorescence intensity (MFI) of POSTN in fibroblasts between paired nontumor and tumor tissues (n=4). ***, $p < 0.001$. (C) Representative IF staining of fibroblasts in tumor and no-tumor tissues. DAPI (blue), α-SMA (green), and POSTN (red), in individual and merged channels are shown. Bar, 50 μm. (D) Kaplan–Meier survival analyses of patients with for low and high infiltration of POSTN$^+$ CAFs in FU-HCC (up), GSE14520 (middle) and TCGA-LIHC (bottom) cohorts.

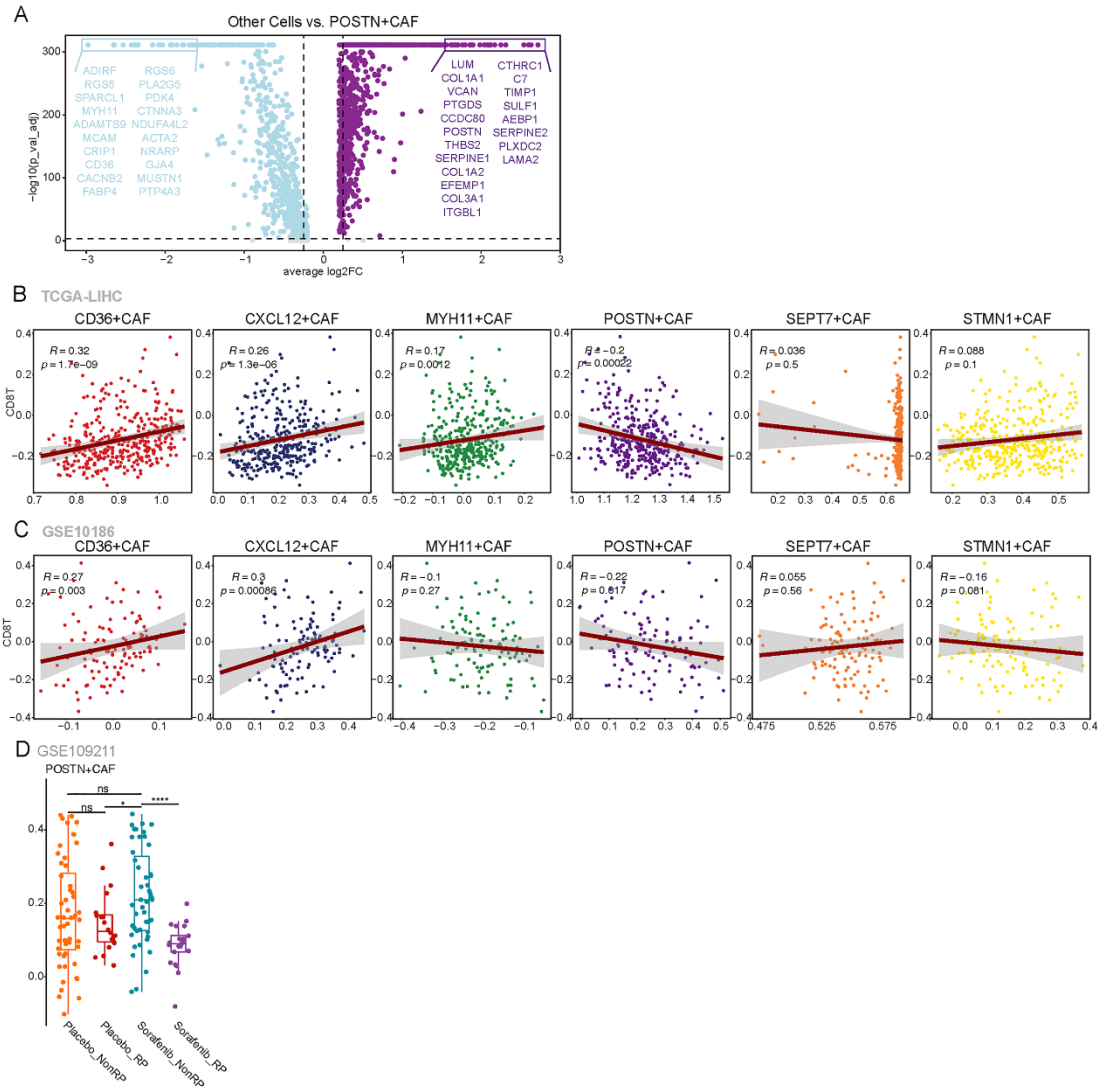

Supplementary Figure 5. The infiltration of POSTN$^+$ CAFs was negatively correlated with that of CD8$^+$ T cells.

(A) Dot plot showing the differential expressed genes between POSTN$^+$ CAFs and other CAFs. The Wilcoxon rank sum test was used to assess the differences. (B-C) Spearman's correlation of the ssGSEA scores of each CAF subtype and CD8$^+$ T cells in TCGA-LIHC cohort (B) and GSE10186 cohort (C). (D) Box plot showing the ssGSEA score of POSTN$^+$ CAFs in different treatment groups in the GSE109211 dataset. The different colors represent different treatment groups.

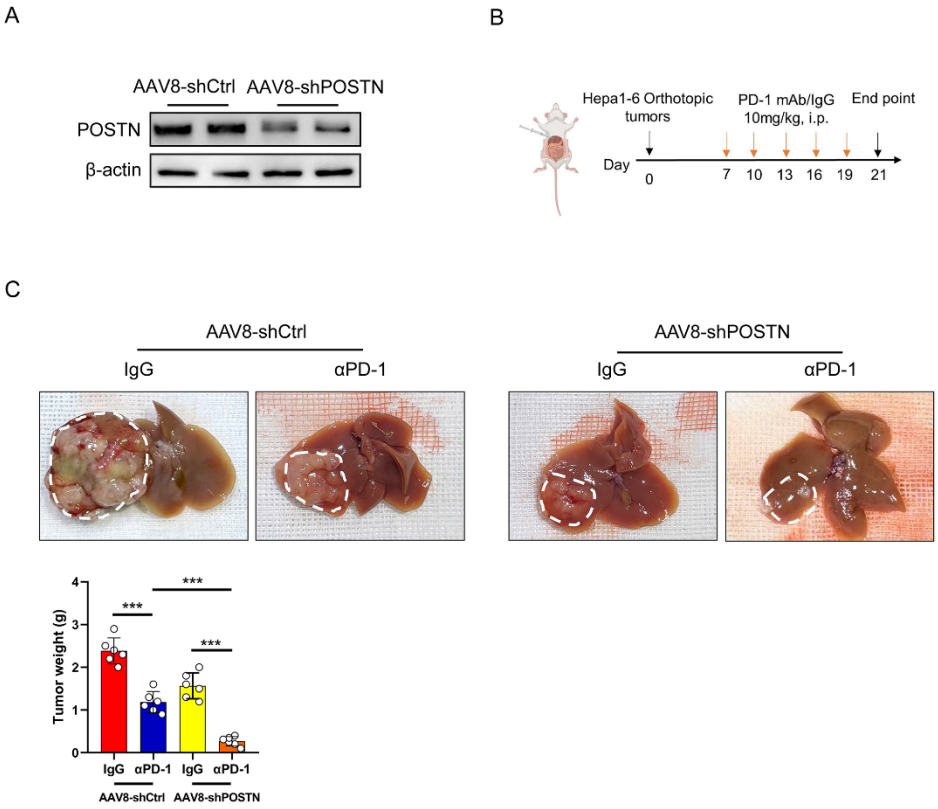

Supplementary Figure 6. Targeting POSTN synergizes with immunotherapy in murine HCC models.

(A) Western blot analysis showing the protein levels of POSTN in the liver of mice treated with AAV8-shPOSTN or AAV8-shCtrl. (B) Schematic view of the treatment plan for orthotopic tumors. C57BL/6 mice treated with AAV8-shCtrl or AAV8-shPOSTN were implanted with Hepa1-6 cells as orthotopic tumors and were treated with an anti-PD-1 mAb or an IgG isotype control. (C) Representative orthotopic tumors obtained after the mice were euthanized (n=6). ***, $p < 0.001$.

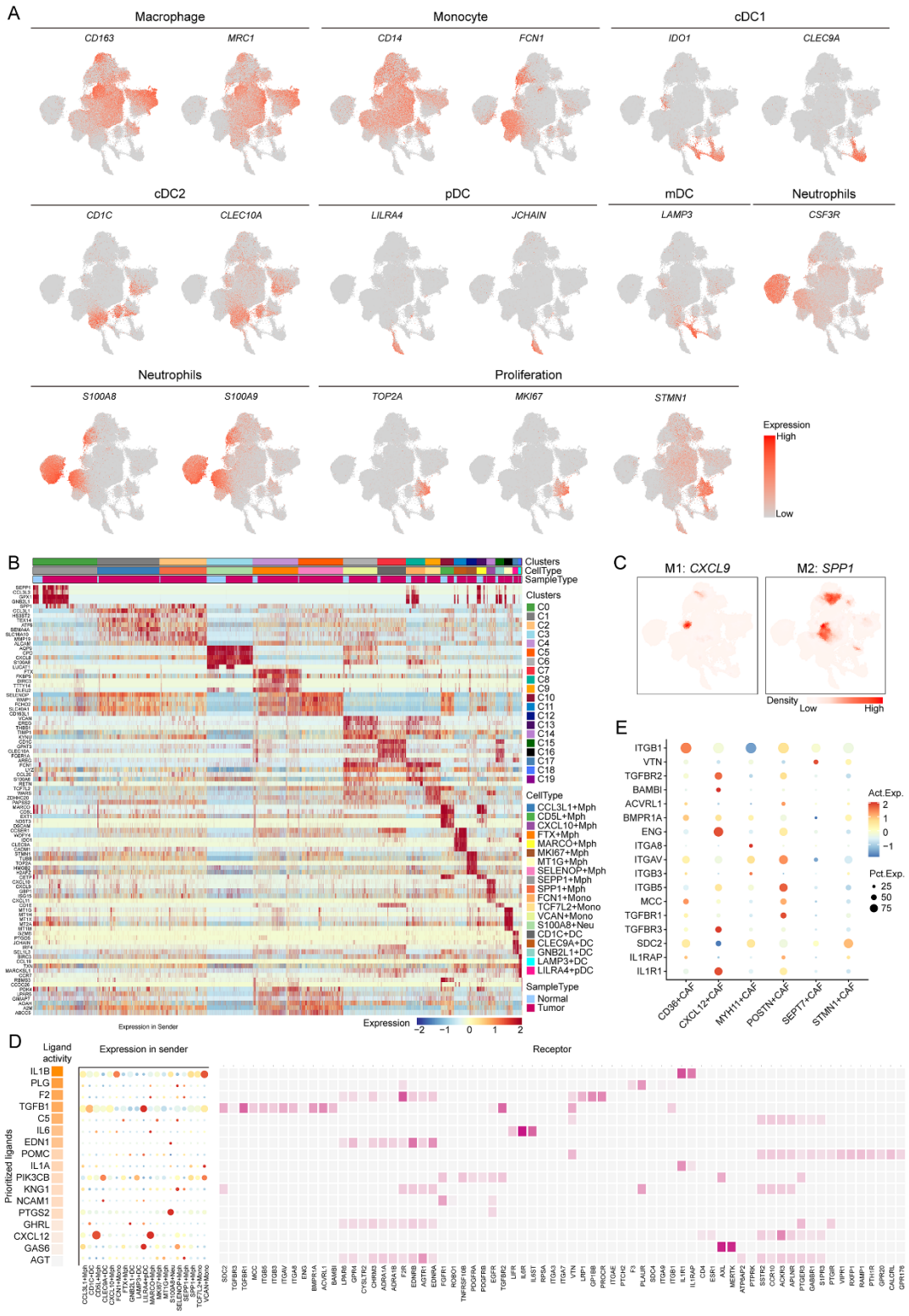

Supplementary Figure 7. Myeloid cells reclustering analysis in HCC.

(A) UMAP plots showing the distribution of genes associated with macrophages (*CD163*, and *MRC1*), monocytes (*CD14*, and *FCN1*), cDC1s (*IDO1*, and *CLEC9A*), cDC2s (*CD1C*, and

CLEC10A), pDCs (*LILRA4*, and *JCHAIN*), mDCs (*LAMP3*), neutrophils (*CSF3R*, *S100A8*, and *S100A9*), and proliferation (*TOP2A*, *MKI67*, and *STMN1*). (B) Heatmap showing the top 5 differential expressed genes in each cell of different myeloid subtypes. (C) UMAP plots showing the density of CXCL9 (M1 marker, left) and SPP1 (M2 marker, right) expression. (D) Top-ranked ligands inferred to regulate $SPP1^+$ macrophages via $POSTN^+$ CAFs according to NicheNet (left). Dot plots showing the expression percentage (dot size) and intensity (dot intensity) of the top-ranked ligands (left) in each CAF subtype (middle). Ligand–receptor pairs showing interactions between $SPP1^+$ macrophages and $POSTN^+$ CAFs ordered by ligand activity (eight). (E) Dot plots showing the percentage (dot size) and intensity (dot intensity) of IL1B or TGFB1-targeted receptors expression in each CAF subtype.

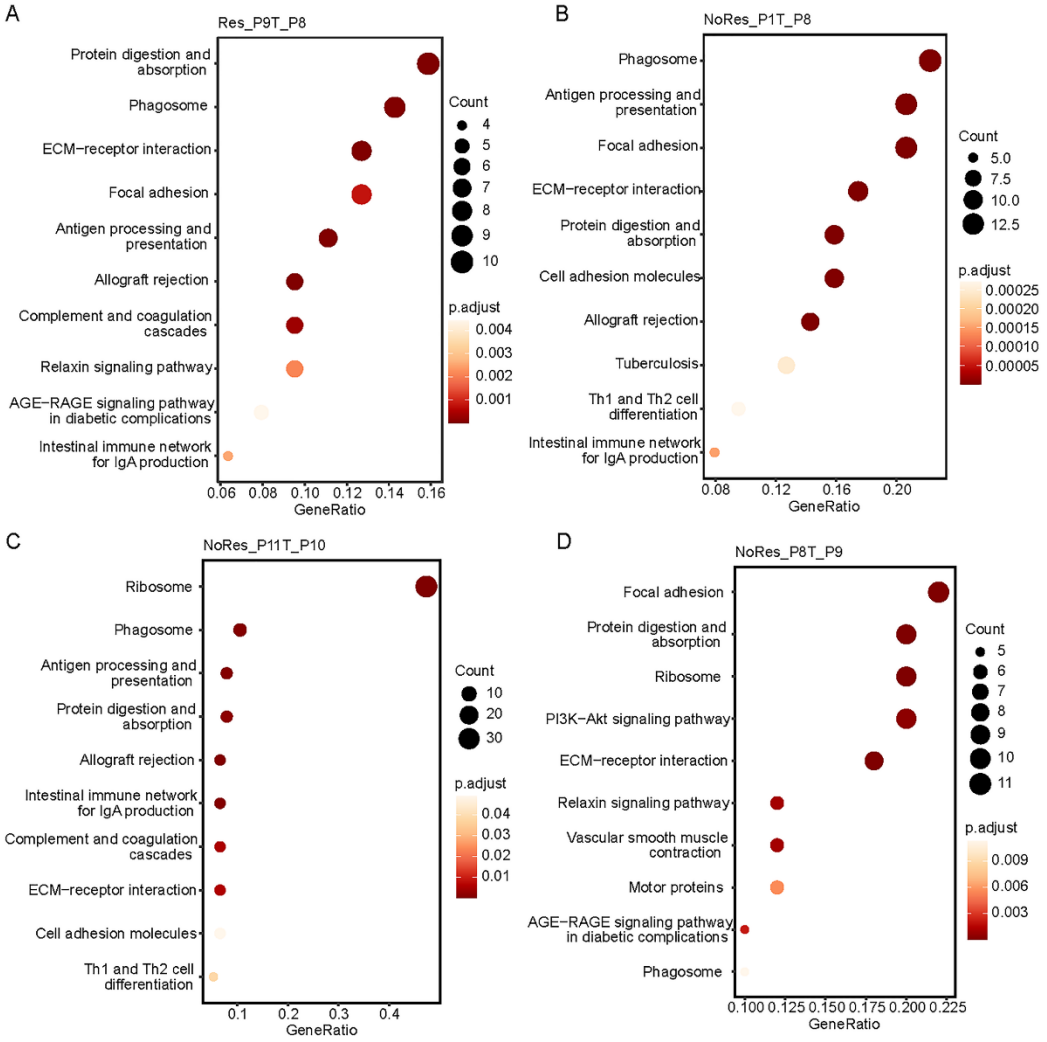

Supplementary Figure 8. Functional enrichment analysis of selected gene programs.

(A-D) Dot plots showing the top 10 enriched pathways in Res_P9T_P8 (A), NoRes_P1T_P8 (B), NoRes_P11T_P10 (C), and NoRes_P8T_P9 (D). The dot size represents the number of enriched genes, and the color represents the adjusted *p* value.

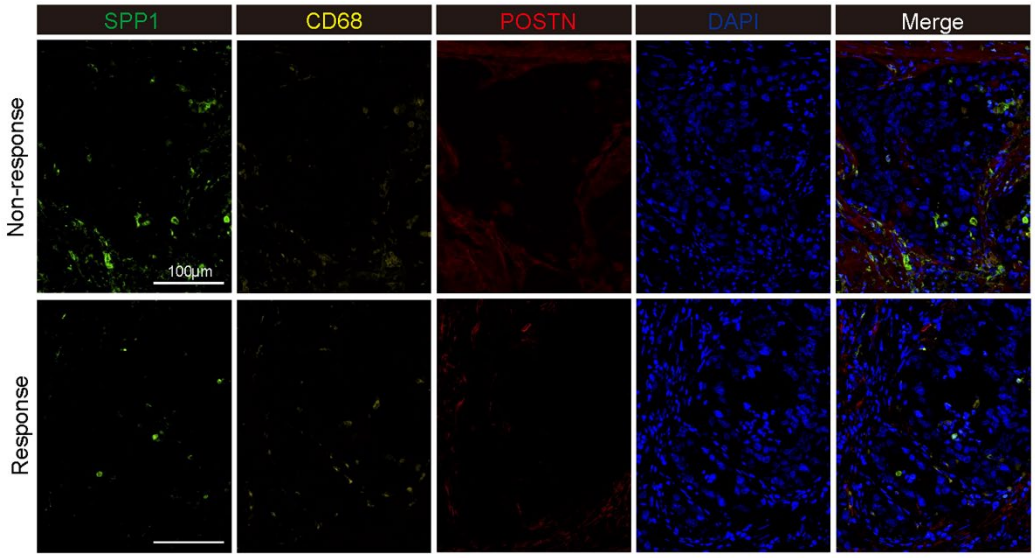

115

116 **Supplementary Figure 9. Response to immunotherapy in HCC patients affected by SPP1$^+$**

117 **macrophages and POSTN$^+$ CAFs.**

118 Representative IF staining of anti-PD1 responder and nonresponder tissues. DAPI (blue), SPP1

119 (green), CD68 (yellow) and POSTN (red) are shown in individual and merged channels. Bar,

120 100 μm.